



## Airborne particles in the city center of Kuala Lumpur: Origin, potential driving factors, and deposition flux in human respiratory airways

Md Firoz Khan<sup>a,\*</sup>, Ahmad Hazuwan Hamid<sup>a</sup>, Md Aynul Bari<sup>b,k</sup>, Abdul Basit Ahmad Tajudin<sup>c</sup>, Mohd Talib Latif<sup>d</sup>, Mohd Shahrul Mohd Nadzir<sup>a,d</sup>, Mazrura Sahani<sup>c,\*</sup>, Muhammad Ikram A. Wahab<sup>c</sup>, Yusri Yusup<sup>e</sup>, Khairul Nizam Abdul Maulud<sup>f,g</sup>, Mohd Famey Yusoff<sup>d</sup>, Nowshad Amin<sup>h</sup>, Md Akhtaruzzaman<sup>i</sup>, Warren Kindzierski<sup>b</sup>, Prashant Kumar<sup>j</sup>

<sup>a</sup> Center for Tropical Climate Change System, Institute of Climate Change, Universiti Kebangsaan Malaysia, 43600 Bangi, Selangor, Malaysia

<sup>b</sup> School of Public Health, University of Alberta, 3-57 South Academic Building, 11405-87 Avenue, Edmonton, Alberta T6G 1C9, Canada

<sup>c</sup> Environmental Health and Industrial Safety Program, Centre for Health and Applied Sciences, Faculty of Health Sciences, Universiti Kebangsaan Malaysia, Jalan Raja Muda Abdul Aziz, 50586 Kuala Lumpur, Malaysia

<sup>d</sup> School of Environmental and Natural Resource Sciences, Faculty of Science and Technology, Universiti Kebangsaan Malaysia, 4300 Bangi, Selangor, Malaysia

<sup>e</sup> Environmental Technology, School of Industrial Technology, Universiti Sains Malaysia, 11800, Pulau Pinang, Malaysia

<sup>f</sup> Earth Observation Center, Institute of Climate Change, Universiti Kebangsaan Malaysia, 43600 Bangi, Selangor, Malaysia

<sup>g</sup> Smart & Sustainable Township Research Centre, Faculty of Engineering and Built Environment, Universiti Kebangsaan Malaysia, 43600 Bangi, Selangor, Malaysia

<sup>h</sup> Institute of Sustainable Energy, Universiti Tenaga Nasional (The National Energy University), Jalan IKRAM-UNITEN, 43000 Kajang, Selangor, Malaysia

<sup>i</sup> Solar Energy Research Institute, Universiti Kebangsaan Malaysia, 43600 Bangi, Selangor, Malaysia

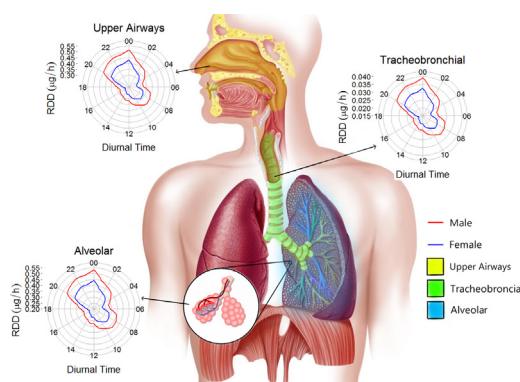
<sup>j</sup> Global Center for Clean Air Research (GCARE), Department of Civil and Environmental Engineering, Faculty of Engineering and Physical Sciences, University of Surrey, Guildford GU2 7XH, Surrey, United Kingdom

<sup>k</sup> Department of Environmental & Sustainable Engineering, College of Engineering and Applied Sciences, University at Albany, State University of New York, Albany, NY 12222, USA

### HIGHLIGHTS

- Particles of  $D_p \leq 0.522 \mu\text{m}$  predominate the particle number concentration (PNC).
- Diurnal of CO and NO coincide with the PNC  $\leq 1 \mu\text{m}$ .
- Local meteorology was found to potentially influence the PNC.
- Transportation, secondary emission and industry were main sources of PNC.
- The deposition flux in the alveolar > upper airways > tracheobronchial for  $\text{PM}_{10}$

### GRAPHICAL ABSTRACT



### ARTICLE INFO

#### Article history:

Received 29 May 2018

Received in revised form 21 August 2018

Accepted 5 September 2018

Available online 7 September 2018

Editor: P. Kassomenos

### ABSTRACT

Equatorial warming conditions in urban areas can influence the particle number concentrations (PNCs), but studies assessing such factors are limited. The aim of this study was to evaluate the level of size-resolved PNCs, their potential deposition rate in the human respiratory system, and probable local and transboundary inputs of PNCs in Kuala Lumpur. Particle size distributions of a 0.34 to 9.02  $\mu\text{m}$  optical-equivalent size range were monitored at a frequency of 60 s between December 2016 and January 2017 using an optical-based compact scanning mobility particle sizer (SMPS). Diurnal and correlation analysis showed that traffic emissions and meteorological

\* Corresponding authors at: Center for Tropical Climate Change System, Institute of Climate Change, Universiti Kebangsaan Malaysia, 43600 Bangi, Selangor, Malaysia.  
E-mail addresses: [mdfiroz.khan@ukm.edu.my](mailto:mdfiroz.khan@ukm.edu.my) mdfiroz.khan@gmail.com (M.F. Khan), [mazrura@ukm.edu.my](mailto:mazrura@ukm.edu.my) (M. Sahani).

**Keywords:**

Urban air pollution  
 Particle number concentration  
 Size distribution  
 Respiratory deposition

confounding factors were potential driving factors for changes in the PNCs ( $D_p \leq 1 \mu\text{m}$ ) at the modeling site. Trajectory modeling showed that a  $\text{PNC} < 100/\text{cm}^3$  was influenced mainly by Indo-China region air masses. On the other hand, a  $\text{PNC} > 100/\text{cm}^3$  was influenced by air masses originating from the Indian Ocean and Indochina regions. Receptor models extracted five potential sources of PNCs: industrial emissions, transportation, aged traffic emissions, miscellaneous sources, and a source of secondary origin coupled with meteorological factors. A respiratory deposition model for male and female receptors predicted that the deposition flux of  $\text{PM}_1$  (particle mass  $\leq 1 \mu\text{m}$ ) into the alveolar (AL) region was higher (0.30 and 0.25  $\mu\text{g}/\text{h}$ , respectively) than the upper airway (UA) (0.29 and 0.24  $\mu\text{g}/\text{h}$ , respectively) and tracheobronchial (TB) regions (0.02  $\mu\text{g}/\text{h}$  for each). However, the  $\text{PM}_{2.5}$  deposition flux was higher in the UA (2.02 and 1.68  $\mu\text{g}/\text{h}$ , respectively) than in the TB (0.18 and 0.15  $\mu\text{g}/\text{h}$ , respectively) and the AL regions (1.09 and 0.91  $\mu\text{g}/\text{h}$ , respectively); a similar pattern was also observed for  $\text{PM}_{10}$ .

© 2018 Elsevier B.V. All rights reserved.

## 1. Introduction

Air pollution due to airborne particulate matter (PM) is an environmental issue in the Southeast Asia (SEA) region, particularly Indonesia, Singapore, Brunei, and Malaysia. Particle pollution from urban activities and transboundary inputs are the most established sources of PM in Malaysia (Khan et al., 2015; Khan et al., 2016a; Latif et al., 2014). Hopke et al. (2008) observed that the overall mean concentration of  $\text{PM}_{10}$  (sum of  $\text{PM}_{2.5-10}$  and  $\text{PM}_{2.5}$ ) was 47.72  $\mu\text{g}/\text{m}^3$  during 2002–2005 in Malaysia under a campaign of the measurement in Asian air quality. Ebihara et al. (2008) also made a measurement of  $\text{PM}_{10}$  in Kuala Lumpur, Malaysia for the year of 2004 and reported that the  $\text{PM}_{10}$  concentration was 43.1  $\mu\text{g}/\text{m}^3$ . In ambient air, heterogeneous atmospheric reactions of reactive gases and gas to particle conversion from primary combustion sources are potential mechanisms to generate particles (Charron and Harrison, 2003; Jang et al., 2002; Limbeck et al., 2003). Local and synoptic scale meteorological factors (e.g., temperature, relative humidity, solar radiation, pressure, and wind speed) are also potential driving factors to enhance the particle number counts (PNCs) in the urban atmosphere (Birmili and Wiedensohler, 2000; Birmili et al., 2001). Atmospheric aerosols can influence climate change by scattering and absorbing radiation, affect the formation of cloud droplets, and lead to decreased visibility (Kumar et al., 2010).

Atmospheric aerosol particles have potentially detrimental effects on human health. Many studies on the health risks of atmospheric aerosols have linked their exposure to increased rates of premature mortality and morbidity during the past 25 years (Cohen et al., 2017; Heal et al., 2012; Lelieveld et al., 2015). For example, a study by Cohen et al. (2017) reported that worldwide deaths attributable to ambient  $\text{PM}_{2.5}$  increased from 3.5 million in 1990 to 4.2 million in 2015. Exposure to ozone ( $\text{O}_3$ ) was estimated to cause an additional 254,000 deaths worldwide and a loss of 4.1 million disability-adjusted life-years from chronic obstructive pulmonary disease. Estimated costs of the health burden of inhalation of  $\text{PM}_{2.5}$  in Seoul are reported to be around USD 1057 million per year for acute exposure and USD 8972 million per year for chronic exposure (Lee et al., 2011). The World Health Organization (WHO) estimated that approximately 3.7 million people worldwide died in 2012 from air pollution (WHO, 2014). This report also suggested that the western Pacific and Southeast Asia regions had the largest count of air pollution hotspots which contributed to approximately 2.6 million deaths.

Air pollution exposure due to high concentrations of aerosol particles (those below 100 nm in diameter) at street level may also severely affect people. Nanoparticles are particles less 100 nm in diameter ( $\text{PM}_{0.1}$ ); these are also referred to as ultrafine particles (Kumar and Goel, 2016). One study suggested a link between the poor health of people living near freeways and power plants and these microscopic air pollutants (Underwood, 2017). Chen et al. (2017) also suggested evidence of a higher risk of dementia for people living near a busy road network. In spite of these human health concerns, nanoparticles have reported beneficial applications; including being used for drug delivery (Kaji et al., 2018), removal of pollutants or preventing environmental

pollution (Gholami et al., 2018; Haghjoo et al., 2018), degradation of pollutants via photocatalysis (Khojasteh et al., 2018; Soofivand et al., 2018), and conversion of energy from one form to another (Soofivand and Salavati-Niasari, 2018). With rapid deterioration in urban air pollution, a quantitative determination of inhaled particles in the respiratory system has yet to be studied near busy urban roadways. Therefore, the focus of this study was to evaluate the level of size-resolved PNCs and their potential deposition rate in different parts of the human respiratory system. Additionally, the aim was to investigate probable local and transboundary sources of the particles.

## 2. Methodology

### 2.1. Description of the sampling site and measurement of the airborne particles

Fig. 1 shows the sampling site located on the rooftop of a three-story building at the Universiti Kebangsaan Malaysia Kuala Lumpur campus (UKM KL). This building faces a busy city road network. The height of the rooftop is approximately 40 m. The land use surrounding the sampling site is shown in Supplement Fig. S1. Transportation comprises the highest land (27.2%) followed by a residential (24%); and commercial, institution and facilities, and open space and recreation lands at 17.6%, 13.6%, and 10.5%, respectively. Other land use comprised of water bodies, industries, infrastructure, and education make up 7.3% combined. A wide range of airborne particles was measured continuously using an Optical Particle Sizer Spectrometer (OPS) (Model 3330, TSI, USA). The instrument operates on the principle of light scattering and can provide an accurate count size distribution for particles in the 0.337 to 9.015  $\mu\text{m}$  range at a sampling frequency of 60 s. Briefly, the OPS uses a laser and a detector to count particles passing through a sensing volume illuminated by the laser. The instrument samples air at a flow rate of 1.0 L/min and can be adjusted by the user. Additionally, 1.0 L/min of sheath flow is also supplied from the exhaust of the pump and is circulated internally. The sheath flow keeps the particles well-focused on the laser light and prevents the optics from getting contaminated. Sheath-air-flow is filtered air that is designed to minimize diffusion losses and to produce a sharp lower cut-off point. Particles pass through the beam, and light scattered by the particles is picked up by an elliptical mirror and focused onto the photodetector. Particle pulses are counted individually and binned into 16 channels (number of channels can be adjusted) based on their pulse heights. The maximum particle size that can be counted is 10  $\mu\text{m}$ . Particles above 10  $\mu\text{m}$  are counted but not sized. The optical equivalent particle size was detected as  $D_p$ . Sampling was conducted from December 7, 2016 to January 3, 2017 using one-minute intervals. The observation data for PNCs were grouped into  $D_p \leq 1 \mu\text{m}$ ,  $D_p \leq 2.5 \mu\text{m}$ , and  $D_p \leq 10 \mu\text{m}$ . PNC data were also converted into particle mass concentrations using OPS built-in software (OPS, 3330, TSI, USA). The PM concentration was grouped as  $\text{PM}_{10}$ ,  $\text{PM}_{2.5}$ , and  $\text{PM}_1$ . Kumar et al. (2010) used the commonly used terminology 'PM' representing "particulate matter" that is used by the regulatory agencies and is also adopted by us in this article.

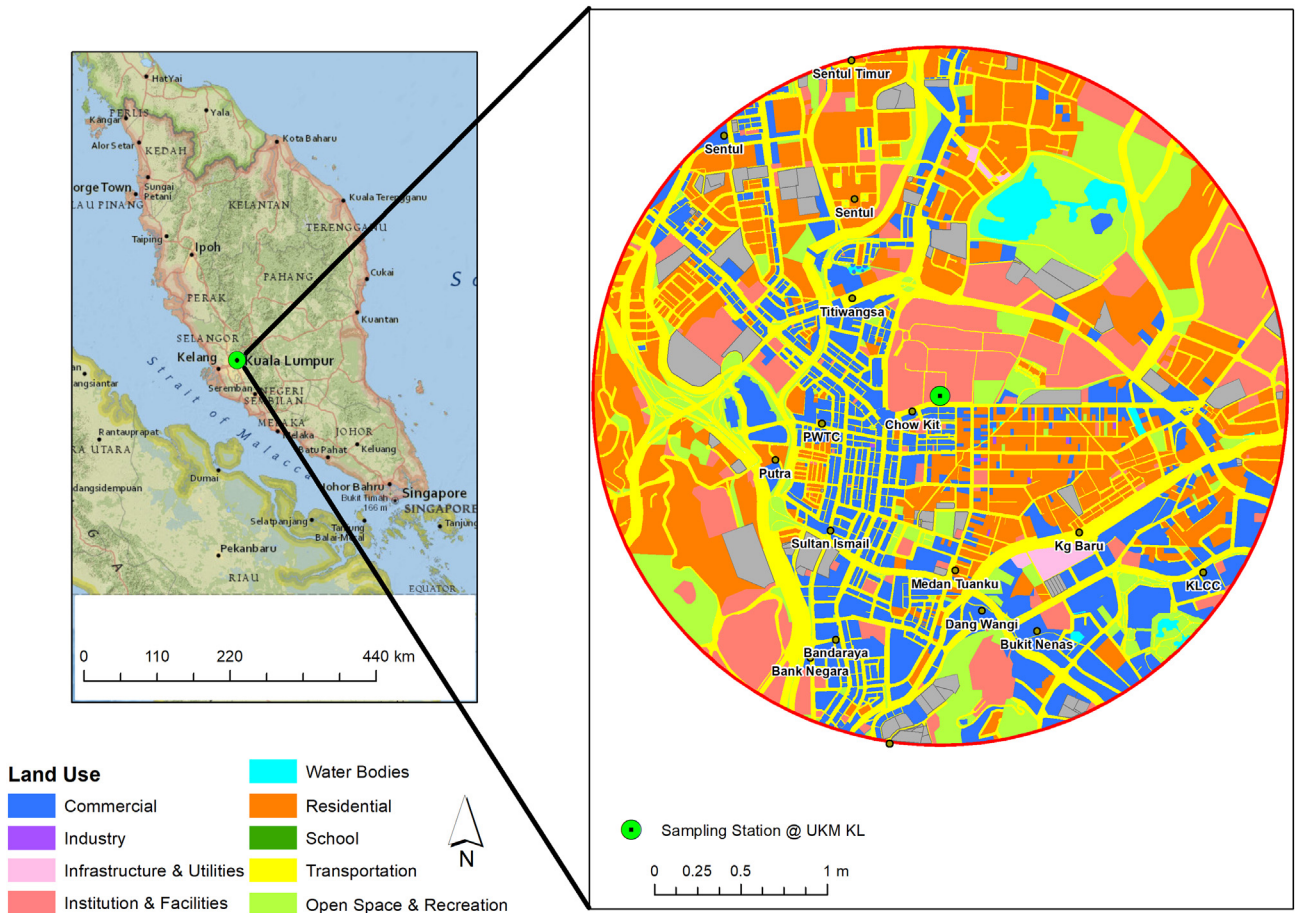


Fig. 1. The study location and the land use in the Kuala Lumpur City of Malaysia.

Other observation data, such as PM<sub>10</sub>, trace gases (O<sub>3</sub>, CO, NO, NO<sub>2</sub>, NO<sub>x</sub>, and SO<sub>2</sub>) and meteorological variables (temperature (T), relative humidity (RH), wind speed (WS), and wind direction (WDir)), were obtained from the Malaysian Department of Environment (DOE) (<http://apims.doe.gov.my/>) and the Malaysian Meteorological Department (MMD) (<http://www.met.gov.my/>), respectively. These data were provided as hourly averages. A comparison of hourly PM<sub>10</sub>-UKMKL versus PM<sub>10</sub>-DOE concentrations was made in Fig. SII. A strong correlation in PM<sub>10</sub> concentrations was observed between these sites. Thus, UKMKL-estimated PM<sub>10</sub> concentrations are reasonably representative of PM<sub>10</sub>-DOE concentrations. However, there was an underestimation in PM<sub>10</sub>-UKMKL versus PM<sub>10</sub>-DOE concentrations. The DOE comparison site (Petaling Jaya in Kuala Lumpur) is located 5 km from the UKMKL site. Differences in the influences of local emission sources, for example, from traffic-industrial emissions close to the monitors, may account for this underestimation as suggested by Amil et al. (2016).

### 2.2. Respiratory deposition dose

Respiratory deposition dose (RDD) was estimated based on the following empirical equation (Eq. (1)) derived from Hinds (1999) for standard atmospheric conditions and a spherical particle size:

$$M_{dep} = \frac{\pi}{6} N \rho_p d_p^3 V_m (DF) \quad (1)$$

where,

M<sub>dep</sub> = the mass of a given particle size deposited in the respiratory system per unit time (μg/h)

N = the number concentration of particle of diameter d<sub>p</sub> (μm) and density ρ<sub>p</sub> (1 g/cm<sup>3</sup>)

V<sub>m</sub> = the inhalation rate (1.5 m<sup>3</sup>/h and 1.25 m<sup>3</sup>/h were applied for males and females, respectively, for light outdoor exercise, as described by the International Commission on Radiological Protection (ICRP) deposition model (ICRP, 1994))

M<sub>p</sub> = the mass of particles (μg)

V<sub>p</sub> = the volume of particles (m<sup>3</sup>)

DF = the deposition fraction of particles (ICRP model only considers diffusional, gravitational, and inertial depositions)

$$\text{Volume of the spherical particle} = \frac{\pi}{6} d_p^3 \quad (2)$$

$$\text{Density equation} = \rho_p = \frac{M_p}{V_p} \quad (3)$$

Substitution of Eq. (2) and Eq. (3) into Eq. (1) (assuming a perfect spherical particle) yields:

$$\begin{aligned} M_{dep} &= \frac{\pi}{6} N \left( \frac{M_p}{V_p} \right) d_p^3 V_m (DF) = \left( \frac{\pi}{6} d_p^3 \right) \left( \frac{M_p}{\frac{\pi}{6} d_p^3} \right) N V_m (DF) \\ &= M_p N V_m (DF) \end{aligned} \quad (4)$$

$$PM = \text{mass}_p \times \frac{\text{count}_p}{\text{volume}} = M_p \times N = \frac{\text{total mass}_p}{\text{volume}} (\mu\text{g}/\text{m}^3) \quad (5)$$

The Eq. (4) was further simplified using Eq. (5) and expressed as Eq. (6):

$$M_{\text{dep}} = \text{PM} \times V_m \times (\text{DF}) \quad (6)$$

DF for upper airways ( $\text{DF}_{\text{UA}}$ ) was estimated for  $\text{PM}_{10}$ ,  $\text{PM}_{2.5}$ ,  $\text{PM}_{2.5-10}$ , and  $\text{PM}_{10}$  using Eq. (7) below as referred by Hinds (1999); Kumar et al. (2017, 2018):

$$\text{DF}_{\text{UA}} = \text{IF} \times \left( \frac{1}{1 + \exp(6.84 + 1.183 \ln d_p)} + \frac{1}{1 + \exp(0.924 - 1.885 \ln d_p)} \right) \quad (7)$$

where IF is the inhalable fraction and can be estimated using the following Eq. (8):

$$\text{IF} = 1 - 0.5 \left( 1 - \frac{1}{1 + 0.00076 d_p^{2.8}} \right) \quad (8)$$

Deposition fraction for the tracheobronchial region (trachea and bronchial airways) as  $\text{DF}_{\text{TB}}$  was estimated using Eq. (9):

$$\text{DF}_{\text{TB}} = \left( \frac{0.00352}{d_p} \right) \left[ \exp(-0.234 (\ln d_p + 3.40)^2) + 63.9 \exp(-0.819 (\ln d_p - 1.61)^2) \right] \quad (9)$$

The deposition fraction of particles for the alveolar region ( $\text{DF}_{\text{AL}}$ ) is:

$$\text{DF}_{\text{AL}} = \left( \frac{0.0155}{d_p} \right) \left[ \exp(-0.416 (\ln d_p + 2.84)^2) + 19.11 \exp(-0.482 (\ln d_p - 1.362)^2) \right] \quad (10)$$

The total deposition fraction (DF) is the sum of the regional deposition and was derived from the aggregate of  $\text{DF}_{\text{UA}}$ ,  $\text{DF}_{\text{TB}}$ , and  $\text{DF}_{\text{AL}}$  during one complete breath for the entire respiratory tract as suggested by Wang (2005).

To estimate  $\text{DF}_{\text{UA}}$ ,  $\text{DF}_{\text{TB}}$ ,  $\text{DF}_{\text{AL}}$ , and IF,  $d_p$  as a mass median optical equivalent diameter (MMD) of  $\text{PM}_{10}$ ,  $\text{PM}_{2.5}$ ,  $\text{PM}_{2.5-10}$ , and  $\text{PM}_{10}$  were derived from the cumulative (%) distribution of the PM concentration, as suggested by Kumar and Goel (2016) (Fig. SIII). However, there is a distinct difference between the optical diameter and aerodynamic diameter and the conversion factor of the optical diameter to the aerodynamic diameter is about twice particularly for coarse particles with irregular shapes and varying densities, as suggested by Chien et al. (2016) and Sanders et al. (2003). In the current study, we did not convert optical diameter to aerodynamic diameter.

### 2.3. Local weather pattern and wind vector

Local and regional wind circulations were visualized using the Grid Analysis and Display System (GrADS) (<http://cola.gmu.edu/grads/>). Surface wind vector (10 m height) and boundary layer height data with a spatial resolution of  $0.25^\circ$  latitude  $\times$   $0.25^\circ$  longitude were obtained from the European Centre for Medium-Range Weather Forecasts (ECMWF) (<https://www.ecmwf.int/en/forecasts/datasets/reanalysis-datasets/era-interim>). Southeast Asian wildfire-related radiative power ( $\text{W}/\text{m}^2$ ) was also obtained to relate to the air particle count. This wildfire data was downloaded from the Monitoring Atmospheric Composition & Climate (MACC) website under ECMWF. MACC provides a fire radiative power (FRP) archive at a spatial resolution of  $0.1^\circ \times 0.1^\circ$ . Note that the rate of thermal radiation release by a fire was related to the rate at which fuel is being consumed and smoke produced from the outdoor fire events. The spatial domain was considered as  $90^\circ\text{E}$  to  $130^\circ\text{E}$  latitude and  $10^\circ\text{S}$  to  $30^\circ\text{N}$  longitude and a monthly mean of wind vector and FRP was determined using the climate data operators (CDO) version 1.6.9 software (<https://code.zmaw.de/projects/cdo>)

developed by the Max Planck Institute. Further, Hybrid Single-Particle Lagrangian Integrated Trajectory version 4.9 (HYSPLIT 4.9) was applied to calculate backward trajectories (Stein et al., 2015). Backtrajectories were calculated for 120 h and 500 m height to represent transport of air masses from transboundary regions and to be free from interference in the atmosphere as reported by Verma et al. (2011). Several other researchers have also applied  $\geq 5$  days and a 500 m starting mixing height of the boundary layer to describe transport of air masses from transboundary regions (Cheng et al., 2015; Khan et al., 2016b; Sahu et al., 2017). Mean clusters were determined for December 2016. Additionally, a wind sector analysis in a form of bivariate analysis was derived. Plots for the regional wind vector, radiative power from wildfires, boundary layer height as well as a cluster of the trajectories are shown in Fig. SIV for December 2016.

### 2.4. Concentration-weighted trajectory (CWT) method

Potential source contribution function (PSCF) analysis is a common method to ascertain the most probable upwind distant source regions. It is widely used to identify regional sources in conjunction with the HYSPLIT model (Bari et al., 2015; Hopke et al., 1995; Pekney et al., 2006). The PSCF values for the grid cells in the study domain are calculated by counting the trajectory segment endpoints that terminate within each cell (Ashbaugh et al., 1985). However, one of the limitations of the PSCF is that the same PSCF values can be observed for grid cells if sample concentrations are slightly higher or extremely higher than the criterion concentrations, making it hard to differentiate large sources from moderate ones. To overcome this limitation of the PSCF, we used the concentration-weighted trajectory (CWT) method, where each grid cell was assigned a weighted concentration by averaging the sample concentrations that have associated trajectories crossing the grid cell as follows (Hsu et al., 2003):

$$C_{ij} = \frac{1}{\sum_{l=1}^M \tau_{ijl}} \sum_{l=1}^M C_l \tau_{ijl} \quad (11)$$

where  $C_{ij}$  is the average weighted concentration in the  $ij^{\text{th}}$  cell,  $l$  is the index of the trajectory,  $M$  is the total number of trajectories,  $C_l$  is the concentration observed on the arrival of trajectory  $l$ , and  $\tau_{ijl}$  is the time spent in the  $ij^{\text{th}}$  cell by trajectory  $l$ . A high value for  $C_{ij}$  implies that air parcels traveling over the  $ij^{\text{th}}$  cell would be, on average, associated with high concentrations at the receptor. In this study, CWT was a function of the receptor model-derived source contributions of different factors and the residence time of a trajectory arriving at the Kuala Lumpur air monitoring station in each grid cell.

It is likely that small values of the number of trajectory segment endpoints that fall in the grid cell ( $n_{ij}$ ) may produce high CWT values with high uncertainties (Polissar et al., 1999). A small number of trajectory segment endpoints (e.g.,  $< 2$ ) can lead to the false identification of upwind and downwind source areas known as the tailing effect due to evenly distributed weight along the path of trajectories (Hsu et al., 2003). As suggested by Polissar et al. (1999), an arbitrary weight function  $W_{ij}$  was multiplied with CWT values to reduce the uncertainty in the values for these cells. The weighting function reduced CWT values when the total number of the endpoints in a particular cell was less than about three times the average value of the end points per cell (PPC). In this case, the empirical weight function  $W_{ij}$  was defined as below based on the literatures (Liu et al., 2013; Xin et al., 2016):

$$W_{ij} = 0.7 \text{ if } \text{PPC} < n_{ij} \leq (3 \times \text{PPC})$$

$$0.42 \text{ if } (0.5 \times \text{PPC}) < n_{ij} \leq \text{PPC}$$

$$0.2 \text{ if } (0.5 \times \text{PPC}) \geq n_{ij}$$

Other uncertainties may exist due to factors unable to be accounted for in the backward trajectory analysis, e.g., an increasing number of trajectory endpoints approaching the receptor location, the distance traveled by single trajectories, turbulent airflows, potential deposition, chemical and physical processes that occur along the trajectory pathway (Chen et al., 2013; Cheng et al., 2015; Stohl, 1998). The details of the CWT and PSCF were visualized in Figs. SV–SVI in the supplementary section.

### 2.5. Positive matrix factorization (PMF) and principal component analysis-absolute principal component score (PCA-APCS) procedures

Identification of the origin of PNC was performed using positive matrix factorization (PMF) and principal component analysis-absolute principal component score (PCA-APCS) procedures. The United States Environmental Protection Agency (USEPA) developed a Windows version of PMF based on the ME-2 engine algorithm by Paatero (1997); Paatero and Tapper (1994). A detailed description of the input file and estimation of the uncertainty was provided by Khan et al. (2016b). For a comparison of the responses of the PMF, the PCA-APCS model proposed by Thurston and Spengler (1985) was applied.

## 3. Results and discussion

### 3.1. Particle number (PNC) concentration and particle mass (PM) concentration

Table 1 and Table SI show hourly and daily particle number concentration (PNC) and concentration of particle mass measured at the optical diameter of 0.34 to 9.02  $\mu\text{m}$  by OPS. This data indicate that PNC was dominated by particles of  $D_p \leq 0.522 \mu\text{m}$  at 96% of the total count. Total PNC was 115/cm<sup>3</sup> measured on an hourly basis for PNC<sub>0.34</sub> to PNC<sub>9.02</sub>.

However, daily value of PNC was 122/cm<sup>3</sup> for this optical diameter range. Comparable data on the measurement of PNC elsewhere is shown in Table SII. Month-long observation of PNC at a semi-urban site of Bangi near Kuala Lumpur in 2013 showed that total PNC was 223/cm<sup>3</sup> in the range of 0.265 to 34  $\mu\text{m}$  (Khan et al., 2015). However, at the rural coast site Bachok, PNC was considerably higher, i.e., 471/cm<sup>3</sup> for the range 0.27 to 4.5  $\mu\text{m}$  (Dominick et al., 2015). PNC data in this study was similar to data in a study conducted in Singapore at a bus stop, highway, and industrial sites. Here PNCs were recorded for the range 0.25 to 32  $\mu\text{m}$ . Their results showed that PNCs were 179, 156, and 228/cm<sup>3</sup> for the bus stop, highway, and industrial sites, respectively (You et al., 2017). A study conducted in Doi Ang Khang in northern Thailand reported PNC as  $10,147 \pm 5800/\text{cm}^3$ . These concentrations were measured by a TSI SMPS in the size range of 13.6–736.5 nm. They identified two biomass burning sources, and no significant local emission sources including from major traffic routes. The high PNC and small geometric mean diameter were observed during biomass fire events (Chuang et al., 2016). Hussein et al. (2014) conducted measurements of PNC in the size range 0.25–32  $\mu\text{m}$  at an urban site in Jeddah, Saudi Arabia during 2011–2012 and total PNCs were  $215 \pm 171/\text{cm}^3$ . Huang et al. (2017) reported that total PNCs were  $0.3 \times 10^4$  to  $2.2 \times 10^4$  and  $0.2 \times 10^4/\text{cm}^3$  at urban and background sites, respectively, in Xiamen, Dongguan, Shenzhen and Hainan, China in the size range 15–615 nm during 2013–2015. Hennig et al. (2018) observed that PNCs were 1437.3/cm<sup>3</sup> in the size range of 100–750 nm during 2009–2014 in a Ruhr background site in Germany. Masiol et al. (2016) reported  $1.1 \times 10^4/\text{cm}^3$  for PNCs in the size range 14 nm–20  $\mu\text{m}$  during April–Jun 2014 at the Po Valley Airport site in Italy. PNC data in the size range >265 nm observed elsewhere was comparable to results of the present study. However, PNCs in the size range <100 nm were higher elsewhere compared to the present study. Likely reasons for differences of PNCs in the present study with the comparison sites in other regions

**Table 1**  
Descriptive statistics of the particle number concentration (PNC) for hourly and daily data.

| Hourly (# cm <sup>-3</sup> ) | N   | Mean   | Geometric | Median | Min   | Max    | 10%   | 90%    | Stdev |
|------------------------------|-----|--------|-----------|--------|-------|--------|-------|--------|-------|
| PNC <sub>0.34</sub>          | 457 | 78.49  | 62.91     | 65.22  | 3.87  | 298.05 | 26.34 | 155.21 | 50.24 |
| PNC <sub>0.42</sub>          | 457 | 24.18  | 17.27     | 16.86  | 0.83  | 127.86 | 6.11  | 60.64  | 21.08 |
| PNC <sub>0.52</sub>          | 457 | 7.39   | 5.09      | 4.96   | 0.28  | 49.56  | 1.81  | 18.47  | 7.42  |
| PNC <sub>0.65</sub>          | 457 | 1.95   | 1.49      | 1.44   | 0.12  | 13.14  | 0.62  | 4.23   | 1.61  |
| PNC <sub>0.81</sub>          | 457 | 1.07   | 0.89      | 0.89   | 0.08  | 6.46   | 0.40  | 2.04   | 0.72  |
| PNC <sub>1.01</sub>          | 457 | 0.51   | 0.43      | 0.44   | 0.04  | 2.35   | 0.21  | 0.93   | 0.30  |
| PNC <sub>1.25</sub>          | 457 | 0.25   | 0.21      | 0.22   | 0.02  | 1.03   | 0.11  | 0.43   | 0.14  |
| PNC <sub>1.56</sub>          | 457 | 0.30   | 0.26      | 0.26   | 0.03  | 1.13   | 0.13  | 0.51   | 0.16  |
| PNC <sub>1.94</sub>          | 457 | 0.36   | 0.31      | 0.31   | 0.03  | 1.88   | 0.16  | 0.63   | 0.21  |
| PNC <sub>2.42</sub>          | 457 | 0.18   | 0.15      | 0.16   | 0.02  | 2.12   | 0.08  | 0.28   | 0.14  |
| PNC <sub>3.01</sub>          | 457 | 0.10   | 0.08      | 0.09   | 0.01  | 2.19   | 0.04  | 0.15   | 0.12  |
| PNC <sub>3.75</sub>          | 457 | 0.06   | 0.05      | 0.05   | 0.01  | 1.55   | 0.02  | 0.08   | 0.09  |
| PNC <sub>4.67</sub>          | 457 | 0.03   | 0.03      | 0.03   | 0.00  | 1.47   | 0.01  | 0.05   | 0.08  |
| PNC <sub>5.82</sub>          | 457 | 0.02   | 0.01      | 0.01   | 0.00  | 1.15   | 0.01  | 0.02   | 0.06  |
| PNC <sub>7.24</sub>          | 457 | 0.01   | 0.01      | 0.01   | 0.00  | 0.78   | 0.00  | 0.01   | 0.04  |
| PNC <sub>9.02</sub>          | 457 | 0.01   | 0.00      | 0.00   | 0.00  | 0.63   | 0.00  | 0.01   | 0.04  |
| PNC <sub>total</sub>         | 457 | 114.89 | 89.97     | 90.01  | 5.36  | 501.13 | 36.56 | 237.73 | 80.60 |
| Daily                        |     |        |           |        |       |        |       |        |       |
| PNC <sub>0.34</sub>          | 23  | 82.17  | 70.40     | 73.55  | 25.32 | 190.99 | 29.40 | 163.11 | 46.93 |
| PNC <sub>0.42</sub>          | 23  | 26.37  | 20.19     | 19.54  | 6.13  | 80.55  | 7.54  | 68.02  | 21.69 |
| PNC <sub>0.52</sub>          | 23  | 8.27   | 6.04      | 5.28   | 1.98  | 28.82  | 2.39  | 22.46  | 7.78  |
| PNC <sub>0.65</sub>          | 23  | 2.13   | 1.72      | 1.58   | 0.65  | 6.30   | 0.84  | 4.78   | 1.59  |
| PNC <sub>0.81</sub>          | 23  | 1.13   | 0.99      | 0.95   | 0.41  | 2.69   | 0.53  | 1.97   | 0.63  |
| PNC <sub>1.01</sub>          | 23  | 0.52   | 0.47      | 0.46   | 0.21  | 1.00   | 0.27  | 0.85   | 0.22  |
| PNC <sub>1.25</sub>          | 23  | 0.25   | 0.23      | 0.24   | 0.11  | 0.43   | 0.13  | 0.41   | 0.10  |
| PNC <sub>1.56</sub>          | 23  | 0.30   | 0.28      | 0.29   | 0.13  | 0.55   | 0.15  | 0.44   | 0.11  |
| PNC <sub>1.94</sub>          | 23  | 0.36   | 0.33      | 0.35   | 0.15  | 0.70   | 0.18  | 0.53   | 0.14  |
| PNC <sub>2.42</sub>          | 23  | 0.18   | 0.17      | 0.17   | 0.08  | 0.29   | 0.11  | 0.27   | 0.06  |
| PNC <sub>3.01</sub>          | 23  | 0.10   | 0.09      | 0.09   | 0.05  | 0.18   | 0.07  | 0.16   | 0.03  |
| PNC <sub>3.75</sub>          | 23  | 0.06   | 0.05      | 0.05   | 0.03  | 0.12   | 0.04  | 0.09   | 0.02  |
| PNC <sub>4.67</sub>          | 23  | 0.03   | 0.03      | 0.03   | 0.02  | 0.09   | 0.02  | 0.05   | 0.02  |
| PNC <sub>5.82</sub>          | 23  | 0.02   | 0.01      | 0.01   | 0.01  | 0.06   | 0.01  | 0.02   | 0.01  |
| PNC <sub>7.24</sub>          | 23  | 0.01   | 0.01      | 0.01   | 0.00  | 0.04   | 0.00  | 0.01   | 0.01  |
| PNC <sub>9.02</sub>          | 23  | 0.01   | 0.01      | 0.00   | 0.00  | 0.03   | 0.00  | 0.01   | 0.01  |
| PNC <sub>total</sub>         | 23  | 121.90 | 101.61    | 103.86 | 35.28 | 312.33 | 41.30 | 262.66 | 78.57 |

are detection methods (light scattering, condensation particle counter, etc.), size range of particles captured and nature of the observation sites.

Mass concentration of PNCs was derived from the number counts are shown in Table SI. Hourly total mass concentration of PNCs represents hourly  $PM_{10}$  and the arithmetic mean of  $PM_{10}$  is  $16.6 \mu\text{g}/\text{m}^3$  as shown in Table 2, while the daily average of the  $PM_{10}$  concentration is nearly same as hourly value. Similarly, the average mass concentration of  $PM_1$  and  $PM_{2.5}$  were  $4.11$  and  $7.63 \mu\text{g}/\text{m}^3$ , respectively. However, Hopke et al. (2008) reported values of  $PM_{2.5-10}$  and  $PM_{2.5}$  of  $18.57 \mu\text{g}/\text{m}^3$  and  $29.15 \mu\text{g}/\text{m}^3$ , respectively, which was observed in Kuala Lumpur during 2002–2005 in a study financed by the World Bank and Asian Development Bank to assess urban air quality in the Asian region. A study by Ebihara et al. (2008) in Kuala Lumpur, Malaysia found concentrations of  $PM_{10}$  obtained from the sum of  $PM_{2.5-10}$  and  $PM_{2.5}$  of  $43.1 \mu\text{g}/\text{m}^3$  for the year of 2004. Begum et al. (2010) observed the concentration  $PM_{2.5-10}$  and  $PM_{2.5}$  were  $44.85 \mu\text{g}/\text{m}^3$  and  $26.22 \mu\text{g}/\text{m}^3$  for the period 2001 to 2005 at the atomic energy center in Dhaka campus. Davy et al. (2011) collected  $PM_{2.5-10}$  and  $PM_{2.5}$  in the capital city of Mongolia for the period 2004–2008 and concentrations of  $PM_{2.5-10}$  and  $PM_{2.5}$  were  $143 \mu\text{g}/\text{m}^3$  and  $46 \mu\text{g}/\text{m}^3$ , respectively.

Concentrations of  $PM_{2.5-10}$  and  $PM_{2.5}$  at current site were far below those observed in other Asian locations. The month-long estimated values of  $PM_{10}$  and  $PM_{2.5}$  from the observation data of PNCs indicates that daily average values were lower than local and other recognized air quality thresholds, e.g., WHO air quality guidelines ( $25 \mu\text{g}/\text{m}^3$  and  $50 \mu\text{g}/\text{m}^3$  for 24 h  $PM_{2.5}$  and  $PM_{10}$ , respectively), USEPA National Ambient Air Quality Standards (NAAQS) ( $35 \mu\text{g}/\text{m}^3$  and  $150 \mu\text{g}/\text{m}^3$  for 24 h  $PM_{2.5}$  and  $PM_{10}$ , respectively), and Malaysian Air Quality Standards ( $75 \mu\text{g}/\text{m}^3$  and  $150 \mu\text{g}/\text{m}^3$  for 24 h  $PM_{2.5}$  and  $PM_{10}$ , respectively).

### 3.2. Impact of potential factors on PNCs at the local and transboundary scale

Observation data for trace gases were obtained from a nearby continuous air quality monitoring station operated by the Malaysian DOE. Diurnal analysis showed distinct patterns in the variations of PNC, PM, and trace gases, such as CO, NO,  $O_3$  and  $NO_2$ . Diurnal patterns of these trace gases help explain the behavior of PNC at the local scale (Figs. 2–4). Two concentration spikes of PNC and PM were observed

between 08:00–10:00 and 18:00–24:00 (all local times). Concentrations of  $PM_{2.5-10}$  and  $PM_{10}$  were more apparent in the period 08:00–10:00 compared to the rest of the day. This result suggests increased mass concentrations of coarse particles ( $PM_{2.5-10}$  and  $PM_{10}$ ) during the morning rush hour. Diurnal patterns of trace gases, particularly CO and NO, representing proxy variables for traffic emissions, coincided with PNCs ( $D_p \leq 1 \mu\text{m}$ ). Similarly,  $SO_2$  follows the trend of PNC ( $D_p \leq 1 \mu\text{m}$ ) indicating emissions from combustion of diesel in heavy vehicles as well as industrial origins. A study conducted in the Hubei province in China with PNC  $D_p \leq 1 \mu\text{m}$  nm observed a consistent diurnal pattern with CO and  $NO_2$  (Zhang et al., 2016). We also observed a spike on Thursday at midnight followed by a small drop at 03:00, which increased at 06:00. A similar pattern was also observed on Friday from midnight until 6 am for both the PNC and PM. We correlated hourly PNC ( $D_p \leq 1 \mu\text{m}$ ) to meteorological factors (T, RH and WS) as confounding variables shown in Fig. 5. A significant negative correlation was observed between PNC counts ( $D_p \leq 1 \mu\text{m}$ ) and WS ( $p < 0.001$ ). Meteorological factors can enhance the diffusion loss of PNCs as observed in a study conducted in China (Zhang et al., 2016). Ambient temperature variations reflect the natural convection process (diurnal heating/cooling) in the boundary layer. The convection process triggers diffusion and dispersion at the surface, which eventually cause losses of PNCs (Tiwari et al., 2014). On the other hand, PNC ( $D_p \leq 1 \mu\text{m}$ ) versus RH showed a positive and significant correlation ( $p < 0.05$ ), suggesting that increasing RH can lead to the generation of the PNC at atmospheric conditions. The effect of RH on PNC is unclear. As observed by Price et al. (2014), RH affects the nucleation of PNC. RH can also influence the condensation loss of PNC. Thus, the linear effect of PNC and RH is difficult to understand.

Most ambient reactive trace gases (CO, NO,  $NO_2$ , and  $SO_2$ ) showed a positive and significant correlation to PNC counts ( $D_p \leq 1 \mu\text{m}$ ) ( $p < 0.05$ ), while  $O_3$  was negatively correlated with PNC counts ( $D_p \leq 1 \mu\text{m}$ ) ( $p = 0.05$ ). Correlation of trace gases with PNC counts ( $D_p \leq 1 \mu\text{m}$ ) suggests that ambient heterogeneous reactions involving trace gases directly or indirectly influenced the level of PNC counts ( $D_p \leq 1 \mu\text{m}$ ), as shown in Fig. 6.  $O_3$  and  $SO_2$  are potential precursors in generating new particles in the ambient atmosphere, although the trend of  $O_3$  was low with respect to PNC counts ( $D_p \leq 1 \mu\text{m}$ ) (Zhang et al., 2017). Other studies also indicate that occurrence of new particles is potentially related to

**Table 2**  
Respiratory deposition dose (RDD) of different PM size for male and female.

|               | $PM_1$ |      |      |      | $PM_{2.5}$ |      |      |       | $PM_{10}$ |      |      |       | $PM_{2.5-10}$ |      |      |       |
|---------------|--------|------|------|------|------------|------|------|-------|-----------|------|------|-------|---------------|------|------|-------|
|               | UA     | TB   | AL   | TD   | UA         | TB   | AL   | TD    | UA        | TB   | AL   | TD    | UA            | TB   | AL   | TD    |
| <b>Male</b>   |        |      |      |      |            |      |      |       |           |      |      |       |               |      |      |       |
| Mean          | 0.37   | 0.03 | 0.39 | 0.79 | 2.37       | 0.21 | 1.27 | 3.85  | 17.8      | 1.52 | 2.55 | 21.89 | 11.5          | 0.62 | 0.81 | 12.94 |
| Geo-mean      | 0.29   | 0.02 | 0.3  | 0.61 | 2.02       | 0.18 | 1.09 | 3.28  | 15.9      | 1.35 | 2.27 | 19.49 | 10.2          | 0.55 | 0.71 | 11.42 |
| Min           | 0.02   | 0    | 0.02 | 0.03 | 0.16       | 0.01 | 0.09 | 0.27  | 2.26      | 0.19 | 0.32 | 2.77  | 1.75          | 0.1  | 0.12 | 1.97  |
| Max           | 1.8    | 0.14 | 1.86 | 3.80 | 9.1        | 0.8  | 4.89 | 14.79 | 67.8      | 5.76 | 9.69 | 83.21 | 64.1          | 3.47 | 4.48 | 72.01 |
| Stdev         | 0.27   | 0.02 | 0.28 | 0.58 | 1.31       | 0.12 | 0.71 | 2.13  | 8.64      | 0.74 | 1.24 | 10.61 | 6.13          | 0.33 | 0.43 | 6.89  |
| 10%           | 0.11   | 0.01 | 0.11 | 0.23 | 0.92       | 0.08 | 0.5  | 1.50  | 8.24      | 0.7  | 1.18 | 10.06 | 5.13          | 0.28 | 0.36 | 5.75  |
| Median        | 0.28   | 0.02 | 0.29 | 0.60 | 2.07       | 0.18 | 1.11 | 3.36  | 16.3      | 1.39 | 2.33 | 20.02 | 11            | 0.59 | 0.77 | 12.31 |
| 90%           | 0.81   | 0.06 | 0.84 | 1.71 | 4.2        | 0.37 | 2.26 | 6.84  | 28.4      | 2.42 | 4.06 | 34.95 | 18.1          | 0.98 | 1.27 | 20.34 |
| Deposited (%) |        |      |      |      | 14         |      |      |       | 34        |      |      |       | 88            |      |      |       |
| Release (%)   |        |      |      |      | 86         |      |      |       | 66        |      |      |       | 12            |      |      |       |
| <b>Female</b> |        |      |      |      |            |      |      |       |           |      |      |       |               |      |      |       |
| Mean          | 0.31   | 0.02 | 0.32 | 0.66 | 1.97       | 0.17 | 1.06 | 3.21  | 14.9      | 1.26 | 2.12 | 18.24 | 9.59          | 0.52 | 0.67 | 10.79 |
| Geo-mean      | 0.24   | 0.02 | 0.25 | 0.51 | 1.68       | 0.15 | 0.91 | 2.74  | 13.2      | 1.12 | 1.89 | 16.24 | 8.47          | 0.46 | 0.59 | 9.52  |
| Min           | 0.01   | 0    | 0.01 | 0.03 | 0.14       | 0.01 | 0.07 | 0.22  | 1.88      | 0.16 | 0.27 | 2.31  | 1.46          | 0.08 | 0.1  | 1.64  |
| Max           | 1.5    | 0.11 | 1.55 | 3.17 | 7.58       | 0.67 | 4.07 | 12.32 | 56.5      | 4.8  | 8.07 | 69.34 | 53.4          | 2.89 | 3.74 | 60.01 |
| Stdev         | 0.23   | 0.02 | 0.24 | 0.48 | 1.09       | 0.1  | 0.59 | 1.78  | 7.2       | 0.61 | 1.03 | 8.85  | 5.11          | 0.28 | 0.36 | 5.74  |
| 10%           | 0.09   | 0.01 | 0.1  | 0.20 | 0.77       | 0.07 | 0.41 | 1.25  | 6.87      | 0.58 | 0.98 | 8.38  | 4.27          | 0.23 | 0.3  | 4.79  |
| Median        | 0.24   | 0.02 | 0.25 | 0.50 | 1.72       | 0.15 | 0.93 | 2.80  | 13.6      | 1.16 | 1.94 | 16.68 | 9.13          | 0.5  | 0.64 | 10.26 |
| 90%           | 0.68   | 0.05 | 0.7  | 1.43 | 3.5        | 0.31 | 1.88 | 5.70  | 23.7      | 2.01 | 3.39 | 29.12 | 15.1          | 0.82 | 1.05 | 16.95 |
| Deposited (%) |        |      |      |      | 14         |      |      |       | 34        |      |      |       | 88            |      |      |       |
| Release (%)   |        |      |      |      | 86         |      |      |       | 66        |      |      |       | 12            |      |      |       |

UA = upper airways; TB = tracheobronchial; AL = alveolar; TD = total deposition.

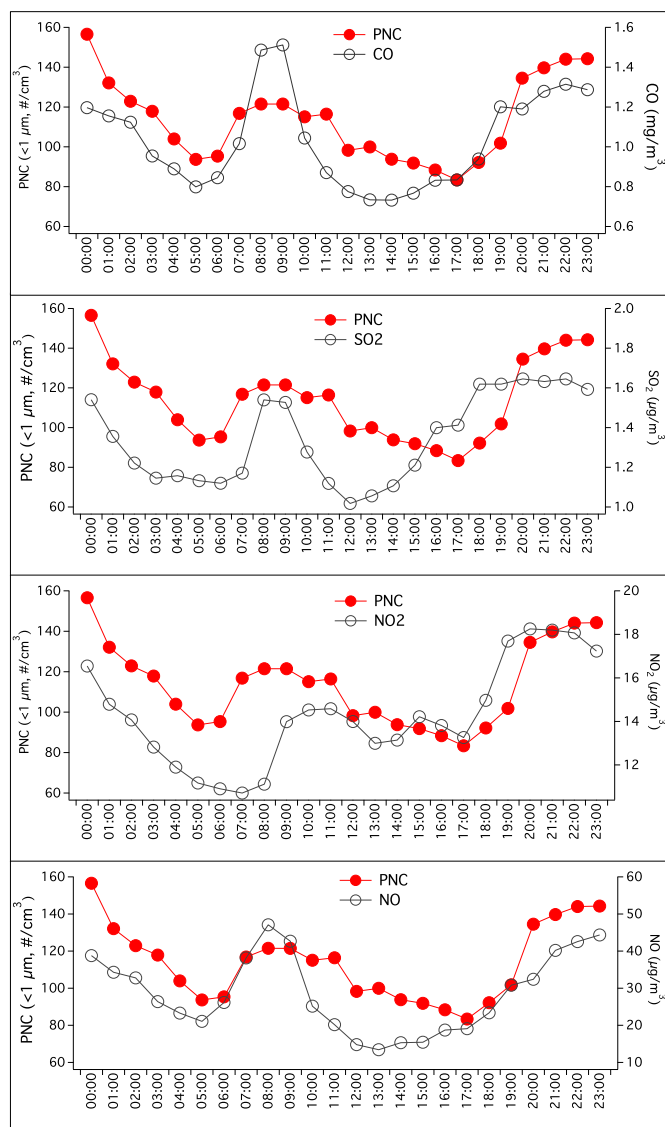


**Fig. 2.** The diurnal variation of PNCs ( $D_p \leq 1 \mu\text{m}$ ) and the key reactive gases (CO, SO<sub>2</sub>, NO and NO<sub>2</sub>).

atmospheric photochemical processes (Andrade et al., 2017; de Almeida Albuquerque et al., 2012). Thus, the above diurnal and correlation analysis provide supporting evidence that local factors influence variations in PNC counts.

Remote transboundary pollution is a potential phenomenon in the SEA region and can affect PNC counts in Kuala Lumpur. Transport of air masses is mainly governed by gradients in atmospheric pressure, which influence the wind speed of a study location. As shown in Fig. SIV of the supplementary section, the predominant air mass originated from the South China Sea as well as Indo-China, bringing polluted and moist air over the Malaysian peninsula region and causing precipitation as well as extreme air pollution events. Our HYSPLIT clustering also showed that pollutant-laden air masses originated from the northeast direction during December 2016. Splitting the trajectories with respect to PNC counts variations demonstrated that  $\text{PNC} < 100/\text{cm}^3$  was influenced mainly from the Indo-China region air mass. However,  $\text{PNC} > 100/\text{cm}^3$  was influenced by air masses originating from both the Indian Ocean and Indo-China regions. Conditional bivariate probability plots, as illustrated in Figs. SVII–SVIII in the supplementary section, showed that  $\text{PNC} (D_p \leq 1 \mu\text{m})$  and  $\text{PNC} (D_p \leq 2.5 \mu\text{m})$  originated from local sources. However, higher wind speeds influenced PNCs originating from the southeast quadrant. Thus, results of conditional bivariate

probability function indicated that PNC counts in the smaller size ranges were influenced greatly by local sources at a lower wind speed. However, PNC counts at a higher wind speed were more affected from the maritime southeast quadrant. Visualization of trajectories weighted with the concentrations of PNC using CWT and PSCF is shown in Figs. SV–SVI. CWT plots for PM<sub>1</sub>, PM<sub>2.5</sub>, and PM<sub>10</sub> indicates that the concentration-weighted air mass was transported mainly from local sources and a northwest direction for  $>4.0 \mu\text{g}/\text{m}^3$ . Air masses from northeast Indochina region resulted in lower concentrations ( $<4.0 \mu\text{g}/\text{m}^3$ ) at the sampling site. Potential source regions for PNCs of  $D_p \leq 1 \mu\text{m}$  were examined using PSCF. The most probable sources were located towards the northwest direction from the sampling sites for PNCs of  $D_p \leq 0.522 \mu\text{m}$ . Thus, consistent results were obtained from HYSPLIT, CWT, and PSCF analysis showing potential air mass influences from the northwest and northeast Indochina region on the level of PNCs.

### 3.3. Source apportionment of PNCs by PMF and PCA-APCS

Fig. 7 and Table SIII show the origin of PNCs determined by PMF and PCA-APCS. PNC observation data coupled with trace gases, ambient temperature, relative humidity and wind speed were applied to the source identification procedures. The purpose of using trace gases and local meteorological factors is to determine their influence on the level of PNCs. PMF extracted five potential factors of PNCs that were associated with several specific source categories: industrial and shipping emissions (Factor 1), combustion from transportation and power generation (Factor 2), aged traffic emissions (Factor 3), miscellaneous sources (Factor 4), and a source of secondary origin coupled with meteorological factors (Factor 5). PCA-APCS also elucidated five factors of PNCs: industrial emissions (PC1), miscellaneous sources (PC2), a source of secondary origin coupled with meteorological factors (PC3), transportation (PC4), and aged traffic emissions (PC5).

Profiles of the factors are similar in nature for both PMF and PCA-APCS analysis despite a shift in the order. Particles originating from industrial and shipping emissions were dominated by the presence of PNCs with an optical diameter ranging from 0.34 to 1.01  $\mu\text{m}$  with a contribution from SO<sub>2</sub>, while aged traffic emissions were dominated by particles with an optical diameter of 1.25 to 1.94  $\mu\text{m}$ . NO<sub>2</sub> was a significant contributor to aged traffic emissions. Similarly, particles with optical sizes of 2.42 to 9.02  $\mu\text{m}$  were abundant in miscellaneous sources where the coarse-mode particles were mainly present. Transportation and power generation sources were identified based on a dominant contribution of CO and NO. On the other hand, O<sub>3</sub> as a secondary trace gas contributed to the secondary origin source. Meteorological factors, such as temperature, relative humidity, and wind speed, were potential contributors to the above source. As this source was influenced by O<sub>3</sub> and meteorological factors, it was classified as a secondary origin coupled with meteorological factors.

Al-Dabbous and Kumar (2015) conducted a source apportionment study of PNCs ranging from 5 to 1000 nm in size in Kuwait using PMF and gaseous pollutants (O<sub>3</sub>, NO, NO<sub>x</sub>, SO<sub>2</sub>, and CO). They observed that approximately 73% of PNCs were attributed to transportation emissions. Similarly, Thimmaiah et al. (2009) observed four major sources of sub-micron aerosol in Prague, Czech Republic, i.e., ozone-rich, NO<sub>x</sub>-rich diesel emissions, traffic and heating sources using PNC, and gaseous and weather input variables for PMF. Salimi et al. (2014) identified a photo-chemically induced source of PNCs in a school environment of the Brisbane Metropolitan area using the K-means clustering technique. These findings suggest that tropical warming conditions and enhanced O<sub>3</sub> levels can contribute to PNCs in Kuala Lumpur. Similarly, traffic emissions, particularly due to the release of CO and NO, are also a potential precursor source of PNCs since the measurement site faces several busy roads in the city.

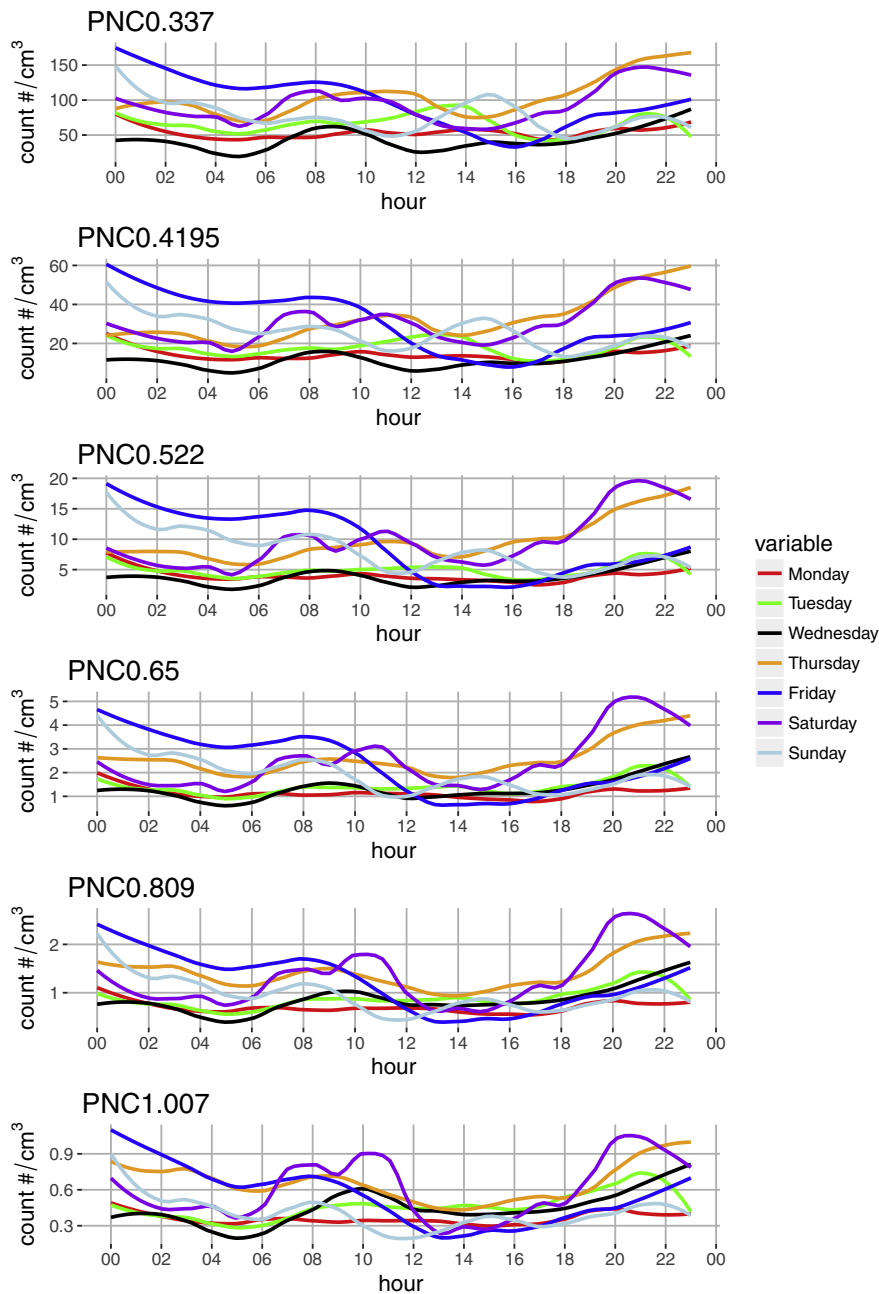


Fig. 3. The diurnal pattern of the PNCs on the days of a week.

### 3.4. RDD

Table 2 shows the predicted deposition of  $PM_{10}$ ,  $PM_{2.5}$ ,  $PM_{2.5-10}$ , and  $PM_{10}$  into human respiratory airways, i.e., UA, TB, and AL deposition for male and female receptors, respectively. As suggested by previous studies (Heyder, 2004; Heyder et al., 1986), diffusional deposition decreases with an increase in particle size of  $1\ \mu m$ . Deposition usually increases with particle size, shape, and density and the period of a respiratory cycle or breathing pattern. Tu et al. (2012) described the functionality of the human respiratory system. The conducting zone (nose to bronchioles) consists of the respiratory organs that form a path to send inhaled air into the deep lung region. The respiratory zone (alveolar duct to alveoli) consists of alveoli and tiny passageways that open into them where gas exchange takes place. Anatomically, the respiratory system can be divided into the upper and lower respiratory tracts.

For  $PM_{10}$ , predicted deposition into the AL region was much higher than into the UA and TB regions for both males and females. However, the difference was distinct after we made a comparison between the TB and AL regions for the  $PM_{2.5}$  and the coarse mode fraction for both male and female receptors. The resulting total deposition (TD) to males was  $0.78\ \mu g/h$  for  $PM_{10}$ ,  $3.50\ \mu g/h$  for  $PM_{2.5}$ ,  $12.70\ \mu g/h$  for  $PM_{2.5-10}$ , and  $22.14\ \mu g/h$  for  $PM_{10}$ , respectively, for males. On the other hand, TD was  $0.65\ \mu g/h$  for  $PM_{10}$ ,  $2.92\ \mu g/h$  for  $PM_{2.5}$ ,  $10.58\ \mu g/h$  for  $PM_{2.5-10}$ , and  $18.45\ \mu g/h$  for  $PM_{10}$ , respectively, for females. Monitoring of air particles at a bus station, highway, and industrial areas in Singapore and human receptor respiratory tract deposition predictions similarly suggested that a large fraction of particles would penetrate deep into the last stage of the respiratory system (You et al., 2017).

Heyder et al. (1986) argued that particle deposition in the upper respiratory tract is governed by inertial impaction due to short residence time and higher velocity. However, in the lower respiratory tract, deposition is mainly influenced by gravitational sedimentation due to low

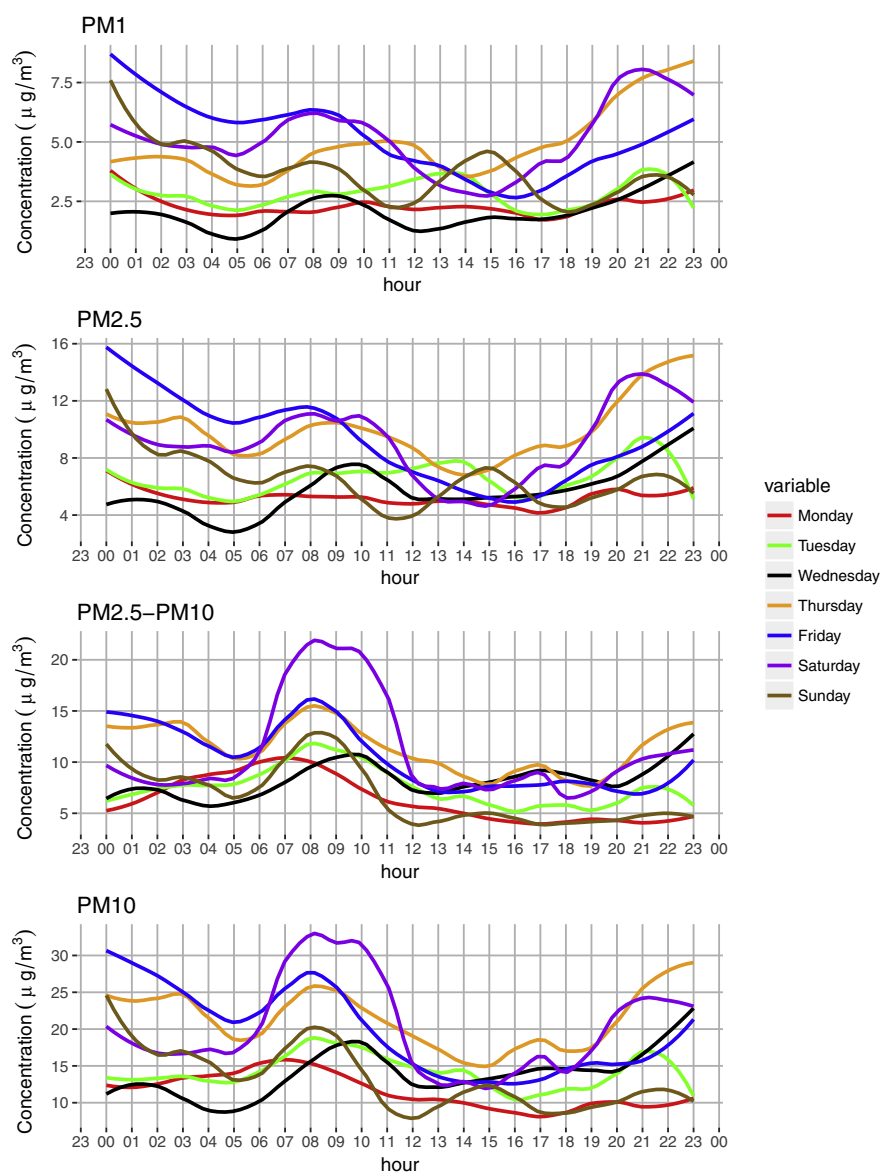


Fig. 4. The diurnal variation of particle mass ( $PM_1$ ,  $PM_{2.5}$ ,  $PM_{2.5-10}$  and  $PM_{10}$ ) on the days of a week.

velocity and long residence time. A study by Lippmann and Albert (1969) introduced particle dynamics in the human system and suggested that deposition by AL decreases for particles larger than  $4\ \mu\text{m}$ . The deposition mechanism is more favorable in the UA and TB airways. A detailed description of the deposition mechanism was provided by Carvalho et al. (2011). They reported that there are five mechanisms that influence particle deposition in the lungs, i.e., inertial impaction, sedimentation, diffusion, interception, and electrostatic precipitation. Among the mechanisms, inertial impaction and sedimentation are directly proportional to particle diameter, while diffusion is inversely related to particle diameter and smaller particles deposit in the lower airways.

Figs. SIX–SX in the supplementary section show predicted diurnal variation of RDD for male and female receptors due to exposure of  $PM_1$ ,  $PM_{2.5}$ ,  $PM_{10}$ , and  $PM_{2.5-10}$ , respectively. The RDD of  $PM_1$  was higher in the AL region for males compared to the UA and TB regions. The predicted deposition flux of the RDD sharply increased during 20:00–00:00 and then gradually decreased until 06:00 in the morning before increasing during morning rush hour at 08:00. Deposition flux went down to the lowest level at 16:00. Predicted deposition of coarse mode particles was influenced more during the morning rush hour than fine mode particles ( $PM_1$  and  $PM_{2.5}$ ). For females, the pattern of

the RDD flux was similar to that of males, but the level of predicted deposition flux was lower in the respiratory system of females than in that of males. From a public health point-of-view, higher deposition of fine mode particles in the AL region from air pollution exposure will be more important for sensitive groups, such as children, compared to adults. As reported by Chuang et al. (2016), children generally breathe more rapidly than adults, spend more time outdoors than adults, and are often more susceptible to health effects of air pollution exposure because their immune systems and developing organs are still immature.

#### 4. Conclusion

This study integrated the measurement data of PNCs with observation data of aerosol, reactive gases and weather variables from local regulatory bodies. Results of the data analysis were interpreted together with trajectory models, estimation of respiratory doses by numerical approximation and multivariate receptor models. Size-resolved PNCs showed that particles in the accumulation mode (optical equivalent diameter  $D_p \leq 0.5\ \mu\text{m}$ ) were the predominant form of PNCs (96%). Diurnal mass concentrations of coarse mode particles ( $PM_{2.5-10}$  and  $PM_{10}$ ) suggest that the emission of the local transportation greatly influence the

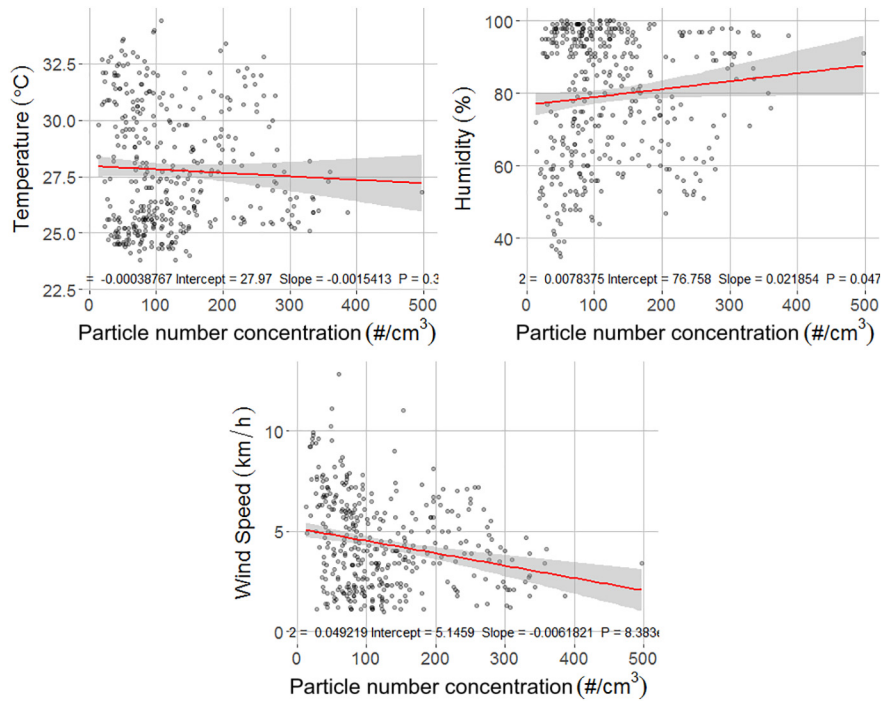


Fig. 5. The correlation plots of the potential weather factors and the PNCs.

level of the coarse particles during the morning rush hour. Results of correlation analysis showed that the PNC level ( $D_p \leq 1 \mu m$ ) declined as WS increased, while an increasing PNC at ambient conditions was correlated to increasing RH. Furthermore, the correlation of trace gases with PNCs ( $D_p \leq 1 \mu m$ ) suggests that ambient heterogeneous reactions of trace gases directly or indirectly influence the level of PNC ( $D_p \leq 1 \mu m$ ). The HYSPLIT trajectory model indicates that a PNC level  $<100/cm^3$  was induced mainly by air masses from the Indochina region. However, a PNC level  $>100/cm^3$  was influenced by air masses originating from both the Indian Ocean and Indochina regions. Conditional bivariate

probability plots showed that the local sources were prominent to PNCs ( $D_p \leq 1 \mu m$ ) and ( $D_p \leq 2.5 \mu m$ ). However, higher wind speeds from the southeast impacted PNCs. Predicted deposition of  $PM_{10}$  into the AL region was much higher than the UA and TB regions for both males and females. However, the predicted deposition flux was much higher in the UA than in the TB and AL regions for  $PM_{2.5}$  and the coarse mode fraction for both male and female receptors. The main sources of PNCs identified by PMF and PCA-APCS were industrial emissions, transportation, aged traffic emissions, miscellaneous sources, and a source of secondary origin coupled with meteorological factors. Tropical warming

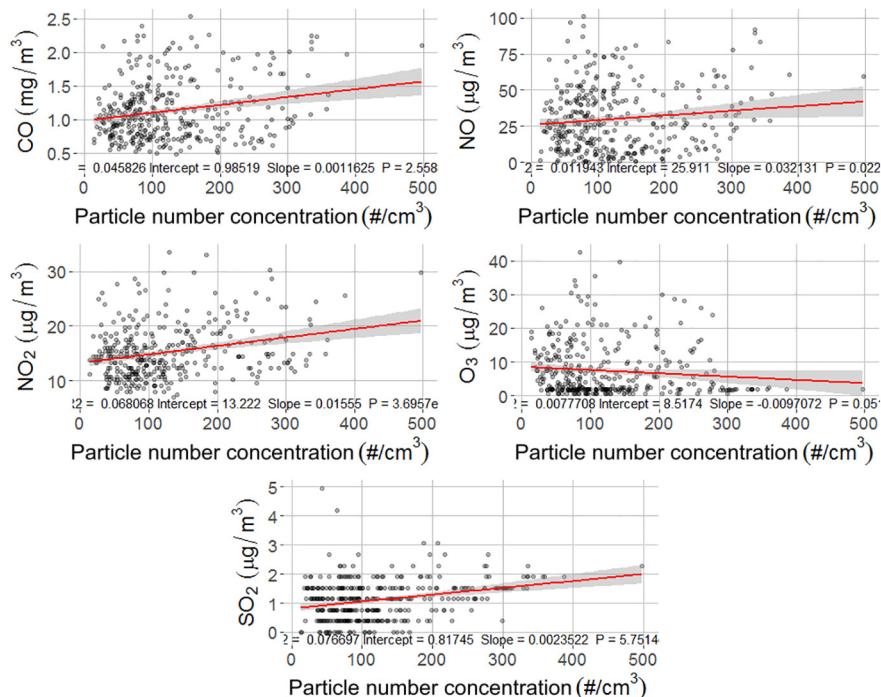


Fig. 6. The correlations of key reactive gases (CO, SO<sub>2</sub>, NO, O<sub>3</sub> and NO<sub>2</sub>) and PNCs.

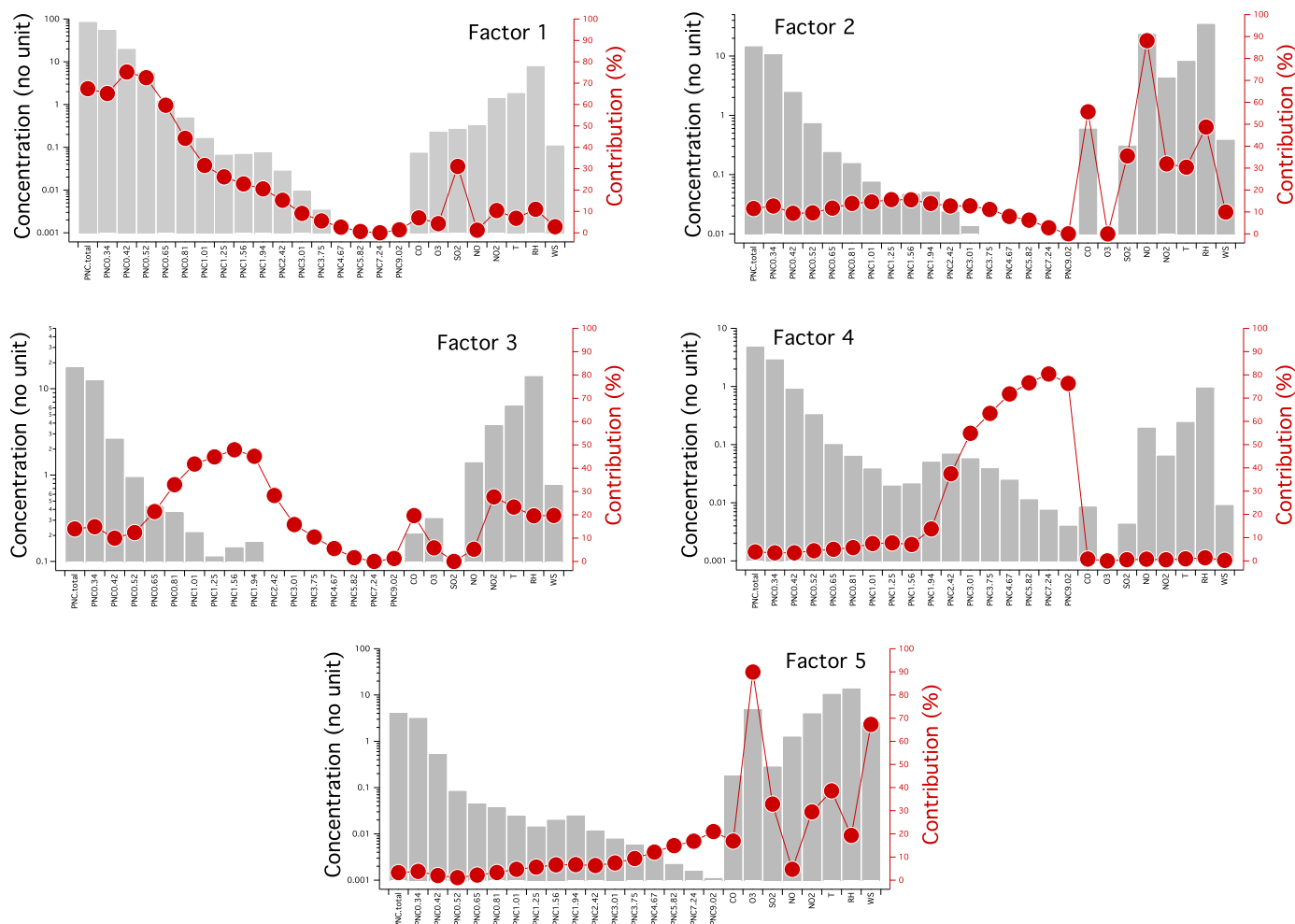


Fig. 7. Source profiles of PNCS by PMF 5.0 expressed as the concentration (no unit) and contribution (%) based on the weight within the factors.

conditions, enhanced  $O_3$  levels and emissions from transportation were identified as potential contributors along with emissions from transportation to PNCS in Kuala Lumpur. The findings of this study can be considered as the baseline PNC data for the under-studied city of Kuala Lumpur. Drawing upon toxicological and aerosol formation points of view, we will focus on ultrafine particles in future research.

### Acknowledgements

The authors would like to thank the Universiti Kebangsaan Malaysia, Malaysia for Research University Grant GGPM-2016-034 and the Ministry of Higher Education, Malaysia for FRGS/1/2017/WAB05/UKM/02/6.

### Conflicts of interests

There are no conflicts of interest to declare.

### Appendix A. Supplementary data

Supplementary data to this article can be found online at <https://doi.org/10.1016/j.scitotenv.2018.09.072>.

### References

Al-Dabbous, A.N., Kumar, P., 2015. Source apportionment of airborne nanoparticles in a Middle Eastern city using positive matrix factorization. *Environ. Sci.: Processes Impacts* 17, 802–812.

- de Almeida Albuquerque, T.T., de Fátima Andrade, M., Ynoue, R.Y., 2012. Characterization of atmospheric aerosols in the city of São Paulo, Brazil: comparisons between polluted and unpolluted periods. *Environ. Monit. Assess.* 184, 969–984.
- Amil, N., Latif, M.T., Khan, M.F., Mohamad, M., 2016. Seasonal variability of  $PM_{2.5}$  composition and sources in the Klang Valley urban-industrial environment. *Atmos. Chem. Phys.* 16, 5357–5381.
- Andrade, M.F., Kumar, P., de Freitas, E.D., Ynoue, R.Y., Martins, J., Martins, L.D., et al., 2017. Air quality in the megacity of São Paulo: evolution over the last 30 years and future perspectives. *Atmos. Environ.* 159, 66–82.
- Ashbaugh, L.L., Malm, W.C., Sadeh, W.Z., 1985. A residence time probability analysis of sulfur concentrations at grand Canyon National Park. *Atmos. Environ.* (1967) 19, 1263–1270.
- Bari, M.A., Kindzierski, W.B., Wallace, L.A., Wheeler, A.J., MacNeill, M., Héroux, M.-È., 2015. Indoor and outdoor levels and sources of submicron particles ( $PM_1$ ) at homes in Edmonton, Canada. *Environ. Sci. Technol.* 49, 6419–6429.
- Begum, B.A., Biswas, S.K., Markwitz, A., Hopke, P.K., 2010. Identification of sources of fine and coarse particulate matter in Dhaka, Bangladesh. *Aerosol Air Qual. Res.* 10, 345–353.
- Birmili, W., Wiedensohler, A., 2000. New particle formation in the continental boundary layer: meteorological and gas phase parameter influence. *Geophys. Res. Lett.* 27, 3325–3328.
- Birmili, W., Wiedensohler, A., Heintzenberg, J., Lehmann, K., 2001. Atmospheric particle number size distribution in central Europe: statistical relations to air masses and meteorology. *J. Geophys. Res.: Atmos.* 106, 32005–32018.
- Carvalho, T.C., Peters, J.L., Williams, R.O., 2011. Influence of particle size on regional lung deposition – what evidence is there? *Int. J. Pharm.* 406, 1–10.
- Charron, A., Harrison, R.M., 2003. Primary particle formation from vehicle emissions during exhaust dilution in the roadside atmosphere. *Atmos. Environ.* 37, 4109–4119.
- Chen, Y., Ebenstein, A., Greenstone, M., Li, H., 2013. Evidence on the impact of sustained exposure to air pollution on life expectancy from China's Huai River policy. *Proc. Natl. Acad. Sci.* 110, 12936–12941.
- Chen, H., Kwong, J.C., Copes, R., Tu, K., Villeneuve, P.J., van Donkelaar, A., et al., 2017. Living near major roads and the incidence of dementia, Parkinson's disease, and multiple sclerosis: a population-based cohort study. *Lancet* 389, 718–726.
- Cheng, L., Xu, X., Zhang, L., 2015. Overview of receptor-based source apportionment studies for speciated atmospheric mercury. *Atmos. Chem. Phys.* 15, 7877–7895.

- Chien, C.-H., Theodore, A., Wu, C.-Y., Hsu, Y.-M., Birky, B., 2016. Upon correlating diameters measured by optical particle counters and aerodynamic particle sizers. *J. Aerosol Sci.* 101, 77–85.
- Chuang, H.-C., Hsiao, T.-C., Wang, S.-H., Tsay, S.-C., Lin, N.-H., 2016. Characterization of particulate matter profiling and alveolar deposition from biomass burning in Northern Thailand: the 7-SEAS study. *Aerosol Air Qual. Res.* 16, 2897–2906.
- Cohen, A.J., Brauer, M., Burnett, R., Anderson, H.R., Frostad, J., Estep, K., et al., 2017. Estimates and 25-year trends of the global burden of disease attributable to ambient air pollution: an analysis of data from the Global Burden of Diseases Study 2015. *Lancet* 389, 1907–1918.
- Davy, P.K., Gunchin, G., Markwitz, A., Trompeter, W.J., Barry, B.J., Shagijamba, D., et al., 2011. Air particulate matter pollution in Ulaanbaatar, Mongolia: determination of composition, source contributions and source locations. *Atmos. Pollut. Res.* 2, 126–137.
- Dominick, D., Latif, M.T., Juneng, L., Khan, M.F., Amil, N., Mead, M.J., et al., 2015. Characterisation of particle mass and number concentration on the east coast of the Malaysian peninsula during the northeast monsoon. *Atmos. Environ.* 117, 187–199.
- Ebihara, M., Chung, Y.S., Dung, H.M., Moon, J.H., Ni, B.-F., Otoshi, T., et al., 2008. Application of NAA to air particulate matter collected at thirteen sampling sites in eight Asian countries: a collaborative study. *J. Radioanal. Nucl. Chem.* 278, 463–467.
- Gholami, T., Salavati-Niasari, M., Sabet, M., 2018. Investigate the effect of silica on improvement electrochemical storage of hydrogen in ZnAl<sub>2</sub>O<sub>4</sub> spinel. *J. Alloys Compd.* 751, 275–282.
- Haghjoo, H., Sangsefidi, F.S., Salavati-Niasari, M., 2018. Synthesis and characterization of Pb<sub>2</sub>SiO<sub>4</sub> nanostructure: study of photo-catalytic behavior of reactive Red198 and reactive Orange16 dyes as pollutants. *J. Mater. Sci. Mater. Electron.* 29, 8002–8009.
- Heal, M.R., Kumar, P., Harrison, R.M., 2012. Particles, air quality, policy and health. *Chem. Soc. Rev.* 41, 6606–6630.
- Hennig, F., Quass, U., Hellack, B., Küpper, M., Kuhlbusch, T.A.J., Stafoggia, M., et al., 2018. Ultrafine and fine particle number and surface area concentrations and daily cause-specific mortality in the Ruhr area, Germany, 2009–2014. *Environ. Health Perspect.* 126 (2), 027008.
- Heyder, J., 2004. Deposition of inhaled particles in the human respiratory tract and consequences for regional targeting in respiratory drug delivery. *Proc. Am. Thorac. Soc.* 1, 315–320.
- Heyder, J., Gebhart, J., Rudolf, G., Schiller, C.F., Stahlhofen, W., 1986. Deposition of particles in the human respiratory tract in the size range 0.005–15 μm. *J. Aerosol Sci.* 17, 811–825.
- Hinds, W.C., 1999. *Aerosol Technology: Properties, Behaviour and Measurement of Airborne Particles*. John Wiley & Sons, UK.
- Hopke, P.K., Barrie, L.A., Li, S.M., Cheng, M.D., Li, C., Xie, Y., 1995. Possible sources and preferred pathways for biogenic and non-sea-salt sulfur for the high Arctic. *J. Geophys. Res.: Atmos.* 100, 16595–16603.
- Hopke, P.K., Cohen, D.D., Begum, B.A., Biswas, S.K., Ni, B., Pandit, G.G., et al., 2008. Urban air quality in the Asian region. *Sci. Total Environ.* 404, 103–112.
- Hsu, Y.-K., Holsen, T.M., Hopke, P.K., 2003. Comparison of hybrid receptor models to locate PCB sources in Chicago. *Atmos. Environ.* 37, 545–562.
- Huang, X., Wang, C., Peng, J., He, L., Cao, L., Zhu, Q., et al., 2017. Characterization of particle number size distribution and new particle formation in Southern China. *J. Environ. Sci. (China)* 51, 342–351.
- Hussein, T., Alghamdi, M.A., Khoder, M., Abdelmaksoud, A.S., Al-Jeelani, H., Goknil, M.K., et al., 2014. Particulate matter and number concentrations of particles larger than 0.25 μm in the urban atmosphere of Jeddah, Saudi Arabia. *Aerosol Air Qual. Res.* 14, 1383–1391.
- ICRP, 1994. International Commission on Radiological Protection, “Human Respiratory Tract Model for Radiological Protection”. *Annals of the ICRP*, Publication 66. Elsevier Science, Inc., Tarrytown, NY.
- Jang, M., Czoschke, N.M., Lee, S., Kamens, R.M., 2002. Heterogeneous atmospheric aerosol production by acid-catalyzed particle-phase reactions. *Science* 298, 814–817.
- Kaji, S.S., Shareghi, B., Bolouki, A., Salavati-Niasari, M., 2018. The effect of TiO<sub>2</sub>-nanoparticle on the activity and stability of trypsin in aqueous medium. *J. Nanostruct.* 8, 168–178.
- Khan, M.F., Latif, M.T., Amil, N., Juneng, L., Mohamad, N., Nadzir, M.S.M., et al., 2015. Characterization and source apportionment of particle number concentration at a semi-urban tropical environment. *Environ. Sci. Pollut. Res.* 22, 13111–13126.
- Khan, M.F., Latif, M.T., Saw, W.H., Amil, N., Nadzir, M.S.M., Sahani, M., et al., 2016a. Fine particulate matter in the tropical environment: monsoonal effects, source apportionment, and health risk assessment. *Atmos. Chem. Phys.* 16, 597–617.
- Khan, M.F., Sulong, N.A., Latif, M.T., Nadzir, M.S.M., Amil, N., Hussain, D.F.M., et al., 2016b. Comprehensive assessment of PM<sub>2.5</sub> physicochemical properties during the Southeast Asia dry season (southwest monsoon). *J. Geophys. Res.: Atmos.* 121, 2016JD025894.
- Khojasteh, H., Salavati-Niasari, M., Sangsefidi, F.S., 2018. Photocatalytic evaluation of RGO/TiO<sub>2</sub>NWs/Pd-Ag nanocomposite as an improved photocatalyst for efficient dye degradation. *J. Alloys Compd.* 746, 611–618.
- Kumar, P., Goel, A., 2016. Concentration dynamics of coarse and fine particulate matter at and around signalised traffic intersections. *Environ. Sci.: Processes Impacts* 18, 1220–1235.
- Kumar, P., Robins, A., Vardoulakis, S., Britter, R., 2010. A review of the characteristics of nanoparticles in the urban atmosphere and the prospects for developing regulatory controls. *Atmos. Environ.* 44, 5035–5052.
- Kumar, P., Rivas, I., Sachdeva, L., 2017. Exposure of in-pram babies to airborne particles during morning drop-in and afternoon pick-up of school children. *Environ. Pollut.* 224, 407–420.
- Kumar, Prashant, Rivas, Ioar, Singh, Anant Pratap, Ganesh, Vikas Julius, Ananya, Monirupa, Frey, H.C., 2018. Dynamics of coarse and fine particles exposure in transport micro-environments. *npj Clim. Atmos. Sci.* 1, 11.
- Latif, M.T., Dominick, D., Ahamad, F., Khan, M.F., Juneng, L., Hamzah, F.M., et al., 2014. Long term assessment of air quality from a background station on the Malaysian Peninsula. *Sci. Total Environ.* 482–483, 336–348.
- Lee, Y.J., Lim, Y.W., Yang, J.Y., Kim, C.S., Shin, Y.C., Shin, D.C., 2011. Evaluating the PM damage cost due to urban air pollution and vehicle emissions in Seoul, Korea. *J. Environ. Manag.* 92, 603–609.
- Lelieveld, J., Evans, J.S., Fnais, M., Giannadaki, D., Pozzer, A., 2015. The contribution of outdoor air pollution sources to premature mortality on a global scale. *Nature* 525, 367.
- Limbeck, A., Kulmala, M., Puxbaum, H., 2003. Secondary organic aerosol formation in the atmosphere via heterogeneous reaction of gaseous isoprene on acidic particles. *Geophys. Res. Lett.* 30, 1996.
- Lippmann, M., Albert, R.E., 1969. The effect of particle size on the regional deposition of inhaled aerosols in the human respiratory tract. *Am. Ind. Hyg. Assoc. J.* 30, 257–275.
- Liu, N., Yu, Y., He, J., Zhao, S., 2013. Integrated modeling of urban-scale pollutant transport: application in a semi-arid urban valley, Northwestern China. *Atmos. Pollut. Res.* 4, 306–314.
- Masiol, M., Vu, T.V., Beddows, D.C.S., Harrison, R.M., 2016. Source apportionment of wide range particle size spectra and black carbon collected at the airport of Venice (Italy). *Atmos. Environ.* 139, 56–74.
- Paatero, P., 1997. Least squares formulation of robust non-negative factor analysis. *Chemom. Intell. Lab. Syst.* 37, 23–35.
- Paatero, P., Tapper, U., 1994. Positive matrix factorization: a non-negative factor model with optimal utilization of error estimates of data values. *Environmetrics* 5, 111–126.
- Pekney, N.J., Davidson, C.L., Zhou, L., Hopke, P.K., 2006. Application of PSCF and CPF to PMF-modeled sources of PM<sub>2.5</sub> in Pittsburgh. *Aerosol Sci. Technol.* 40, 952–961.
- Polissar, A.V., Hopke, P.K., Paatero, P., Kaufmann, Y.J., Hall, D.K., Bodhaine, B.A., et al., 1999. The aerosol at Barrow, Alaska: long-term trends and source locations. *Atmos. Environ.* 33, 2441–2458.
- Price, H.D., Arthur, R., Bérubé, K.A., Jones, T.P., 2014. Linking particle number concentration (PNC), meteorology and traffic variables in a UK street canyon. *Atmos. Res.* 147–148, 133–144.
- Sahu, L.K., Tripathi, N., Yadav, R., 2017. Contribution of biogenic and photochemical sources to ambient VOCs during winter to summer transition at a semi-arid urban site in India. *Environ. Pollut.* 229, 595–606.
- Salimi, F., Ristovski, Z., Mazaheri, M., Laiman, R., Crilley, L.R., He, C., et al., 2014. Assessment and application of clustering techniques to atmospheric particle number size distribution for the purpose of source apportionment. *Atmos. Chem. Phys.* 14, 11883–11892.
- Sanders, P.G., Xu, N., Dalka, T.M., Maricq, M.M., 2003. Airborne brake wear debris: size distributions, composition, and a comparison of dynamometer and vehicle tests. *Environ. Sci. Technol.* 37, 4060–4069.
- Soofivand, F., Salavati-Niasari, M., 2018. “Ag<sub>2</sub>HgI<sub>4</sub>” a thermochromic compound with superionic conducting properties: synthesis, characterization and investigation of graphene-based nanocomposites. *J. Mol. Liq.* 252, 112–120.
- Soofivand, F., Esmaeili, E., Sabet, M., Salavati-Niasari, M., 2018. Simple synthesis, characterization and investigation of photocatalytic activity of NiS<sub>2</sub> nanoparticles using new precursors by hydrothermal method. *J. Mater. Sci. Mater. Electron.* 29, 858–865.
- Stein, A.F., Draxler, R.R., Rolph, G.D., Stunder, B.J.B., Cohen, M.D., Ngan, F., 2015. NOAA’s HYSPLIT atmospheric transport and dispersion modeling system. *Bull. Am. Meteorol. Soc.* 96, 2059–2077.
- Stohl, A., 1998. Computation, accuracy and applications of trajectories—a review and bibliography. *Atmos. Environ.* 32, 947–966.
- Thimmaiah, D., Hovorka, J., Hopke, P.K., 2009. Source apportionment of winter submicron Prague aerosols from combined particle number size distribution and gaseous composition data. *Aerosol Air Qual. Res.* 9, 209–236.
- Thurston, G.D., Spengler, J.D., 1985. A quantitative assessment of source contributions to inhalable particulate matter pollution in metropolitan Boston. *Atmos. Environ.* (1967) 19, 9–25.
- Tiwari, S., Bisht, D.S., Srivastava, A.K., Pipal, A.S., Taneja, A., Srivastava, M.K., et al., 2014. Variability in atmospheric particulates and meteorological effects on their mass concentrations over Delhi, India. *Atmos. Res.* 145–146, 45–56.
- Tu, J., Inthavong, K., Ahmadi, G., 2012. *Computational Fluid and Particle Dynamics in the Human Respiratory System*. Springer Science & Business Media.
- Underwood, E., 2017. The polluted brain. *Science* 355, 342–345.
- Verma, R.L., Kondo, Y., Oshima, N., Matsui, H., Kita, K., Sahu, L.K., et al., 2011. Seasonal variations of the transport of black carbon and carbon monoxide from the Asian continent to the western Pacific in the boundary layer. *J. Geophys. Res.: Atmos.* 116.
- Wang, C.-S., 2005. Chapter 9 deposition models. In: Wang, C.-S. (Ed.), *Interface Science and Technology*. 5. Elsevier, pp. 127–148.
- WHO, 2014. *Ambient (Outdoor) Air Quality and Health*.
- Xin, Y., Wang, G., Chen, L., 2016. Identification of long-range transport pathways and potential sources of PM<sub>10</sub> in Tibetan plateau uplift area: case study of Xining, China in 2014. *Aerosol Air Qual. Res.* 16, 1044–1054.
- You, S., Yao, Z., Dai, Y., Wang, C.-H., 2017. A comparison of PM exposure related to emission hotspots in a hot and humid urban environment: concentrations, compositions, respiratory deposition, and potential health risks. *Sci. Total Environ.* 599–600, 464–473.
- Zhang, T., Zhu, Z., Gong, W., Xiang, H., Li, Y., Cui, Z., 2016. Characteristics of ultrafine particles and their relationships with meteorological factors and trace gases in Wuhan, Central China. *Atmos. Environ.* 7, 96.
- Zhang, X., Yin, Y., Lin, Z., Han, Y., Hao, J., Yuan, L., et al., 2017. Observation of aerosol number size distribution and new particle formation at a mountainous site in Southeast China. *Sci. Total Environ.* 575, 309–320.